New method to characterize aerodynamic flow state around wind turbine blades

Dimitri Voisin[1], Didier Velayoudon[1], Matteo Capaldo[2], John-Richard Ordonnez-Valera[2], Rachel Jorand[3], Mohammed Fajar[2]

5 [1]BladeSENSE, 5 quai E, Concarneau, 29900, France
[2]TotalEnergies OneTech, 2 place Jean Millier, 92078 Paris La Défense cedex, France
[3]CVA Engineering, Avenue Larribau, 64018 Pau cedex, France

Correspondence to: Dimitri Voisin (dvoisin@bladesense.fr)

10 **Abstract.** This paper presents a novel methodology for characterizing the aerodynamic flow state around wind turbine blades, with the aim of optimizing blade aerodynamics to maximize energy production and extend turbine service life. The study leverages advanced eTellTale (eTT) sensors, deployed on two Vestas V27 wind turbines at the SWIFT Facilities (Sandia National Laboratory, Texas), to analyze the relationship between the flow condition on blade suction sides and output power. Results demonstrate that attached flow states increase energy production
15 by 15% compared to the average energy production, while detached flows result in a 30% reduction compared to average energy production. The eTT sensor data, correlated with high-frequency meteorological measurements, enables differentiation of power output curves in attached versus detached aerodynamic regimes. The findings indicate that 15% of potential power is lost during 33% of operational time under low and medium wind conditions due to flow detachment. The methodology is further validated through wind tunnel experiments linking eTT
20 signals to lift coefficient and angle of attack, establishing a strong correlation between sensor data and power output. The approach provides actionable insights for future real-time turbine control, with implications for increasing efficiency and meeting global wind energy targets.

1 Introduction

The recent GWEC report (GWEC 2025) describes that 2024 saw another record-breaking year for wind energy,
25 with 117 GW of new capacity installed globally. Rather than simply marking a slight increase from the previous year, this report highlights an industry expanding to new territories, the rise of promising wind energy hubs, and technological advancements that are meeting the growing demand for reliable, clean electricity in an increasingly unpredictable world. Given the right conditions, the wind industry can accelerate its growth, aiming for the 320 GW required to achieve the targets set at COP28.

30 One approach to boosting the energy output from wind turbines is to increase the size of their rotors—a trend that has gained momentum in recent years, though it brings its own set of challenges (GWEC 2025). Alternatively, enhancing the efficiency of wind turbines themselves offers another path forward. While it is always true that the Betz limit sets an upper bound on the amount of wind energy that can be converted into electrical power, current wind turbine technologies still fall short of this theoretical maximum. Improving efficiency within these constraints
35 remains an important frontier for innovation in the wind industry.

Additionally, the power coefficient related to the rotor design often does not match the values observed once the wind turbine is in operation (Kumar, et al., 2022). Existing models still fall short of accurately reflecting real-

world conditions, particularly because turbulence remains a highly complex phenomenon that is difficult to understand and model.

40 The power produced by the rotor in below rated wind speed is directly related to the wind power available. The power coefficient, is a key factor in this relationship and should be optimized to achieve the highest possible output. In modern wind turbines that allow adjustments to both speed and blade pitch, the efficiency depends on two main factors: the ratio of the rotor tip speed to the wind speed, and the angle at which the blades are pitched. There is an ideal ratio and an ideal pitch angle that will yield the maximum efficiency and, as a result, the most

45 power.

In actual practice, when the wind is below the rated speed, operators maintain a constant, ideal blade pitch while adjusting the rotor speed to keep the optimal ratio between tip speed and wind speed, even as the wind changes. These ideal settings may vary from those suggested by the manufacturer due to local aerodynamic effects and other influences unique to each site. Over time, the best settings can also change because of blade wear, different

50 weather conditions, and other factors. To address these challenges, in literature can be find the Extremum Seeking Control (Creaby et al., 2009) and more recently the Log-Power Proportional-Integral Extremum Seeking (Kumar et al., 2022).

The aim of this study is to experiment a new approach to optimize the aerodynamics of wind turbine blades to maximize production revenues and extend service lifetime. The analysis of the wind turbine power curve was

55 conducted as a function of the flow condition on the suction side of a wind turbine blade.

A test campaign was conducted in 2024 at the SWIFT Facilities (Sandia National Laboratory -Texas USA) to test the eTellTale's sensor (eTT) capabilities in real conditions on 2 wind turbines to analyse the power curve.

1.1 State of the art

Blade response to turbulence shows distinct trends under three scale ranges (Gao et al., 2020). The blade structure

60 responds strongly to the turbulent inflow in the lower and intermediate ranges, while it is primarily dominated by the rotation effect and other high-frequency characteristics of the turbine in higher frequencies.

The small timescales from small turbulent structures generated in a wind turbine wake for instance (Chamorro et al., 2012), have a strong impact on blade loads (Bartholomay et al., 2018). Anemometers measure at the wind turbine nacelle is not sufficient to characterize the state of the flow on the aerodynamic surfaces (attached/

65 detached, laminar/transitional or turbulent aerodynamic boundary layer), which is critical to optimize production performances.

Another issue is the effect of aerodynamic imbalance due to individual blade pitch angle misalignment, which has a significant impact on the remaining useful life of wind turbines which is well known (Saathoff et al., 2021). Blade misalignment measurements were carried out using a laser-optical method, showing that 38% of 195 wind

70 turbines were misaligned. The solution to extend the life of wind turbines is correcting the pitch misalignments. Aerodynamic imbalance not only diminishes energy production efficiency but also exacerbates structural vibrations, induces rotor speed variations, and elevates loads across multiple turbine components, thereby reducing the overall operational lifespan of the turbine (Hyers et al., 2006; Elosegui et al., 2018; Astolfi, 2019). Furthermore, Kusnick et al. (2015) established that even a minor pitch misalignment in a single blade can lead to a significant

75 increase in main shaft loading.

Sensors are a response to mitigate those problematics and become essential for experimental testing, validating design choices and simulation models (Veers et al., 2023). Advanced measurement campaigns have been conducted, but high-quality data is still lacking. There is a need to develop new autonomous measurement systems for large-scale turbines. Advanced real-time measurement systems are required to better capture unsteadiness and non-linearity of fluid flow around the blades, monitor aerodynamic loads and structural responses for better performances of wind turbines.

1.2 Panel of existing sensors for the blade

1.2.1 Internal sensors

Strain sensors measure the local strains and can be used to measure the blade root bending moment.

Fiber optic sensors for wind turbine blades are a proven technology for structural health monitoring (SHM) and load measurement, especially because they integrate well with composite blades (fiberglass or carbon fiber). They use optical fibers (often embedded during manufacturing or bonded to the surface) to sense strain, temperature, vibration, and sometimes acoustic events.

Inertial sensors for a wind turbine blade are used to measure motion, orientation, and vibration to improve control, monitoring, and fault detection. They typically fall under Inertial Measurement Units (IMUs), which combine accelerometers, gyroscopes, and sometimes magnetometers. Mounted at the root blade for structural monitoring or at mid-span or near tip to detect aerodynamic loads and dynamic behavior.

1.2.1 Inflow sensors

Inflow sensors measure local aerodynamic conditions on a blade section, allowing local loads. Common local sensors include **pitot tubes** achieve good accuracy (Ezzeddine et al., 2019), they require regular maintenance and calibration (prone to vibration, contamination, and weather effects) and **surface pressure sensors** (expensive, fragile, and clog-prone). Remote inflow sensors (e.g., lidar) and nacelle-mounted sensors (e.g., spinner anemometers) are alternatives.

Blades as the sensors of the flow to measure the blade loads (Coquelet et al., 2024) is also a solution. This estimation of the incoming wind conditions based on the blade bending moments can be used as an estimator to activate the control strategy on the turbine.

Digital tuft flow visualization with high definition camera have been tested to understand the resulting three-dimensional and transient aerodynamics effects on a 10m diameter two-blade 25kW wind turbine (Nigel et al., 2016). Digital tuft flow visualization allows to know the fraction of tufts (number of stall acrylic yarn tufts vs number of tufts on the outer suction side of the blade) exhibiting detached flow (stall). The independently measured instantaneous turbine output power production correlates highly with the stall fraction. Digital tuft allows to follow dynamic stall and stall hysteresis on the azimuthal variation causing potentially by vertical wind shear. Hence the trailing of the tufts is very useful from an aerodynamic point of view, but industrial implementation is complicated. The e-TellTale sensor to detect flow separation based on strain gage technologies have shown ability in wind tunnel to detect flow separation (Soulier et al., 2022). However, the sensor is mechanically fragile, which causes measurements to drift over time, meaning that it cannot provide absolute measurements. Furthermore, it drifts with temperature.

2 Methods

In this study, we use a set of aerodynamic sensors eTT providing mean and standard deviation raw data to
characterise the state of the flow whether it is attached or detached.

The goal of the study is also to test an algorithm to get an estimation of AoA and loads on wind turbine blades.
The algorithm integrates applied mathematical techniques to transform sensors raw data in terms of aerodynamical
physical properties. These applied mathematical methods need to be trained in a wind tunnel.

2.1 eTT sensor description

eTellTale's sensor (eTT) is a wireless aerodynamic stall sensor based on hall effect figure (1) each composed of a
silicone strip. It is glued on the blade's suction side to qualify the inflow behaviour on the blade (detached or
attached) in real time at 200Hz with filtering standard deviation of magnetic field Bz (Tesla 10^{-3}).

The signal was then recorded with the same acquisition frequency as for the pressure measurements in the wind
tunnel.

Figure 1 – eTT sensors

2.2 eTellTale calibration in wind tunnel at full scale

The experiments were conducted in the 5 m x 6 m high-speed wind tunnel in CSTB Nantes (see figure 2 and
Neunaber et al, 2022 for further details). Its turbulent intensity level is less than 3%. The airfoil profile has been
scanned on a real wind turbine blade (Senvion 2 MW) at 80% from the blade root.

The overall aerodynamic forces on the airfoil profile were measured with 2 rings pressure tape.

The experimentation allows to set thresholds for the standard deviation for eTT to detect detached and attached
flow behaviour.

And finally, wind tunnel experimentation using a machine learning method to link eTT values to AoA and lift
force. The training was carried out on 4 eTTs sensors at 15% chord.

- The reduced model is conducted for -5° < AoA < 22° and wind speed of 20m/s to 40m/s
- The large model is conducted for -5° < AoA < 30° and wind speed of 20m/s to 40m/s

Outside this range of AoA and wind speed, a linearization is applied.
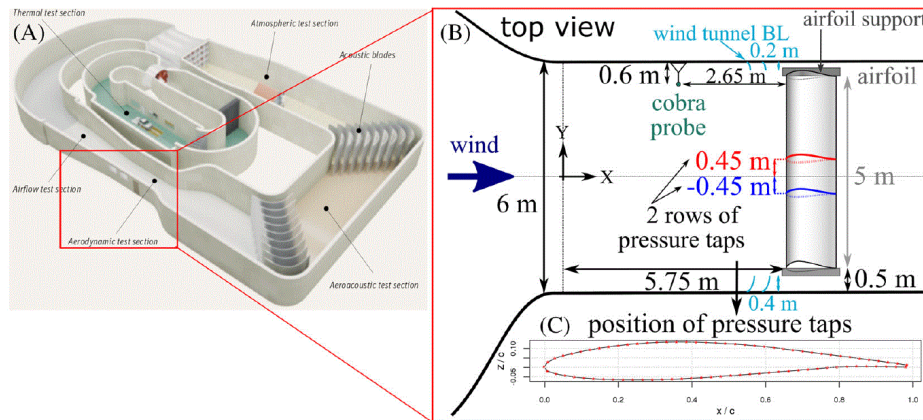
Figure 2 - Wind tunnel set up (Neunaber et al, 2022)

140

Figure 3 - Wind tunnel set up in 2024

Figure 4a,b shows mean and standard deviation (STD) lift versus AoA, while figure 4c shows the eTT signal with its standard deviation in the filled area.

The variations in the magnetic field are directly related to the movements of the eTT silicon tell, and therefore to

145 its sensitivity to disturbances in the flow.

Statistical processing of each component of the magnetic flux density vector yields the standard deviation obtained for each experiment. A filter according to the Z component (normal to the wall) is used to obtain the polar curves in Figure 4c.

A learning process is then used to link lift and AoA to the magnetic flux density vector on the Z axis and to wind

150 speed in Figure 5.

(a)

(b)

(c)
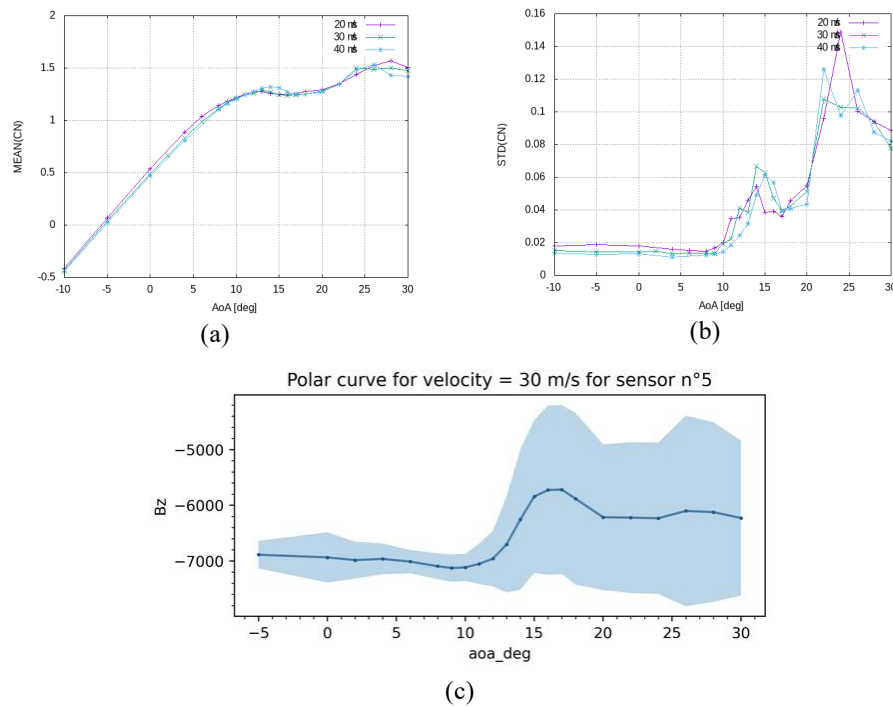
Figure 4 - eTT raw signal and CN
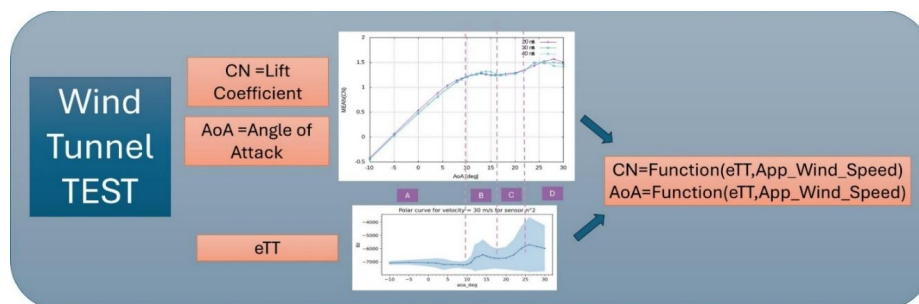
Figure 5 - machine learning method to get lift coefficient and Angle Of Attack

2.3 Description of the field tests

155 The experimentation has been conducted at the SWIFT infrastructure of the Sandia National Laboratory (SNL - Texas) facilities on two wind turbine generators (Vestas V27) called A1 and A2.

To correct the power curve meteorological parameters (Cup31 BP27m Temp27m RH27m) have been measured from a meteorological tower METa1.

Figure 6 - SWIFT Facilities SNL Texas USA

2.3.1 Power correction according to weather conditions

The output Generated Power (GenPwr) has been corrected with the weight of the air. The corrected Generated Power (GenPwr_Cor) is necessary to enable comparison with the theoretical power curve of Vestas and to make possible a comparison in the time.

$$\rho = \frac{1}{Rs.(273{,}15 + Temp27m)} \left(BP27m - 230{,}617.RH27m.e^{\frac{(17{,}5043*Temp27m)}{241{,}2+Temp27m}} \right)$$

With

$BP27m$: Barometric pressure at 27m tower height (Pascal)

$RH27m$: Relative humidity at 27m tower height (%)

$Temp27m$: Air temperature at 27m tower height (°C)

Rs: Dry air Constant 287,06 J kg^{-1} K^{-1}

$$GenPwr_{Cor} = \frac{1.225}{\rho} GenPwr$$

With

$GenPwr$: Generator power measured by variable frequency drive (full power converter) (KW)

ρ: Air Density (kg/m3)

2.3.2 Power curve corrected and split method

The SWIFT Facilities gives the opportunity to have access to high frequency meteo mast data (time-averaging on 0.1s for True Wind Speed, True Wind Direction, Pressure, Temperature and Relative Humidity). The correction of generated power is possible to get a GenPower corrected on each wind turbine. The correction is necessary to compare with the V27 theoretical power curve provided by Vestas.
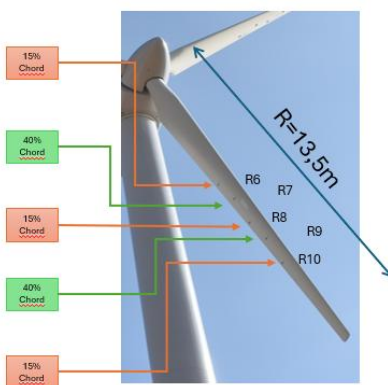
180

Radius :Length from the blade root	% chord from trailing edge	Chord length	eTT Location from trailing edge
6m	15%	93cm	14cm
7m	40%	90cm	36cm
8m	15%	80cm	12cm
9m	40%	75cm	30cm
10m	15%	67cm	10cm

Figure 7 – eTT position on Vestas V27

At the same time, the eTT sensors provide raw data on 5 positions on the blade's suction side (figure 7) in such a way that it is possible to differentiate the corrected GenPower curve in Detached and Attached behaviors.

185 Power Loss criteria is defined to get the difference between Detached and Attached in term of time % and identifies the potential increase of production (figure 8).
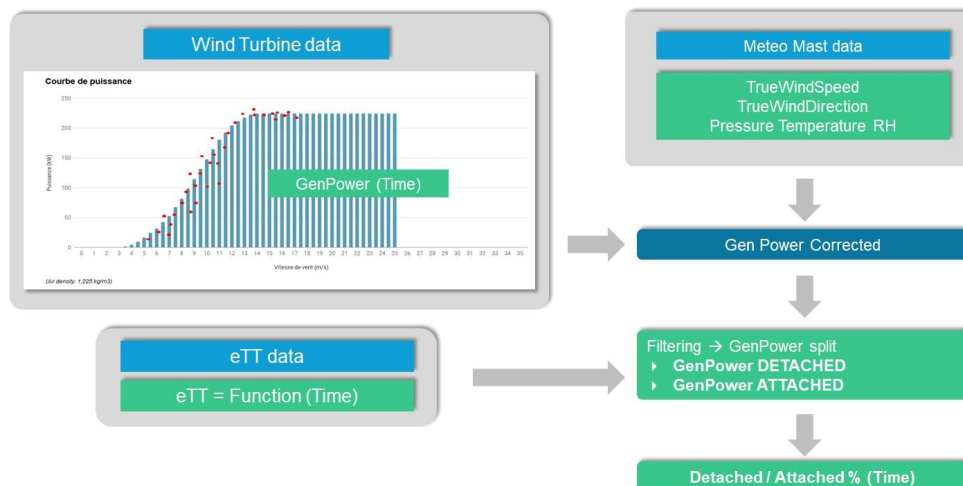
Figure 8 – Power curve corrected method

3 Results

3.1 Pitch Distribution for A1 & A2

190

During August September and October 2024 and January 2025 about 20 days of experimentation on wind turbines A1 and A2 have been conducted. In summary, 1545 hours on A1 and 610 hours on A2.

Different offset of pitch angle have been tested for wind turbine A1 and A2 (figure 9):

- A1 Pitch offset of -3°, -2° -1°, 0°, +1°, +2°, +3°, +4°, +5°

195
- A2 Pitch offset of 0° and +1°

Pitch angle of 1° is the reference value for these 2 wind turbines corresponding to the 0° reference value to reach the optimum TSR in the standard control algorithm of the wind turbine.
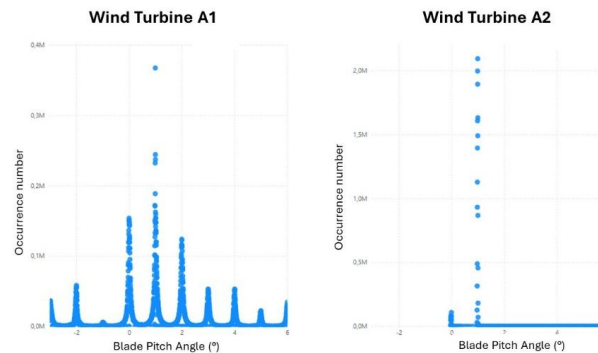
Figure 9 – Blade pitch distribution for A1 & A2

200

3.2 Power Curve measures analysis for A1 & A2

The power curve is plotted on Figure 10 , 11, 12 and 13 for the A1 and A2 wind turbines at +1° of pitch angle (reference value for optimum TSR). The power curve is plotted on Figure 14 for A1 at -3°, A1 at +1° and A2 at +1°.

205
For A1 in the range 4.5-7.5 m/s it is observed that when the flow is attached at eTT R9 the power is much higher than for the measured power curve (figure 10). There is then a great potential (around 59%) increase power for A1 at +1° of pitch if the flow is attached at R9. From wind speed v=7,5 m/s the measured power curve converges with the attached values and there is no potential increase. This corresponds to a chaotic behavior of R9 that we call "hard stall".

210
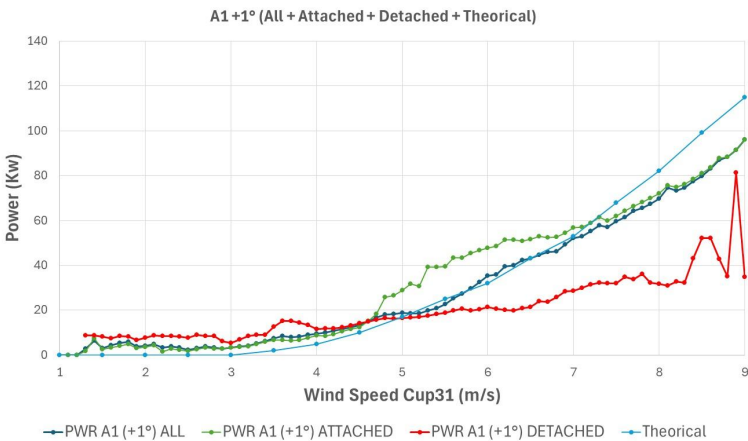
Wind Speed	PWR A1 (+1°) ALL	PWR A1 (+1°) ATTACHED	PWR A1 (+1°) DETACHED	GAIN
(m/s)	(KW)	(KW)	(KW)	
5,2	18,5	30,6	19,8	65%
5,7	27,3	43,4	20,5	59%
6,7	45,8	52,4	23,8	14%

Figure 10 - A1(pitch +1°) power curve filtering according to the Attached / Detached criteria

The same applies for A2 where there is also great potential for increasing power (figure 11) up to wind speed v=7,5 m/s. From wind speed v=7,5 m/s the measured power curve converges with the attached values and there is no

215 potential increase unlike A1. The same chaotic behavior of R9 ("hard stall") is observed.
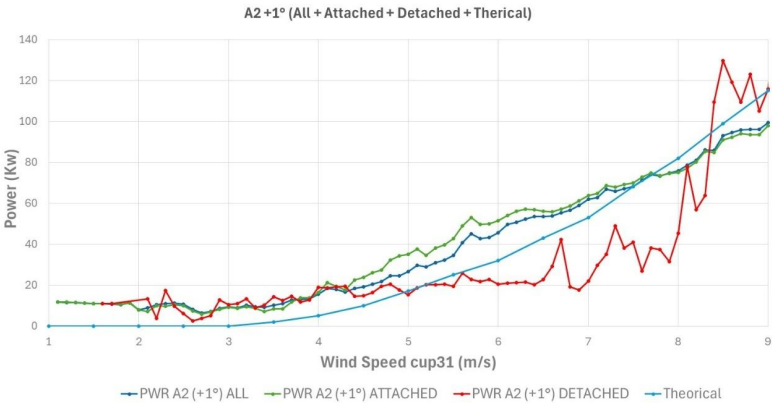
Wind Speed	PWR A2 (+1°) ALL	PWR A2 (+1°) ATTACHED	PWR A2 (+1°) DETACHED	GAIN
(m/s)	(KW)	(KW)	(KW)	
5,2	26,6	35,2	21,8	32%
5,7	44,9	52,9	22,7	18%
6,7	55,4	57,0	40,9	3%

Figure 11 - A2(pitch +1°) power curve filtering according to the Attached / Detached criteria

Nevertheless, the potential increase is much higher for A1 than for A2. A2 seems to have better performance than

220 A1. This is confirmed by comparing A1 and A2 power curves where A2 produces more than A1 (figure 12) for wind speed greater than 4.5 m/s.

Wind Speed	PWR A1 (+1°) ALL	PWR A2 (+1°) ALL	GAIN
(m/s)	(KW)	(KW)	
4,5	13,5	19,0	41%
5,5	22,8	34,6	52%
6	35,4	45,4	29%
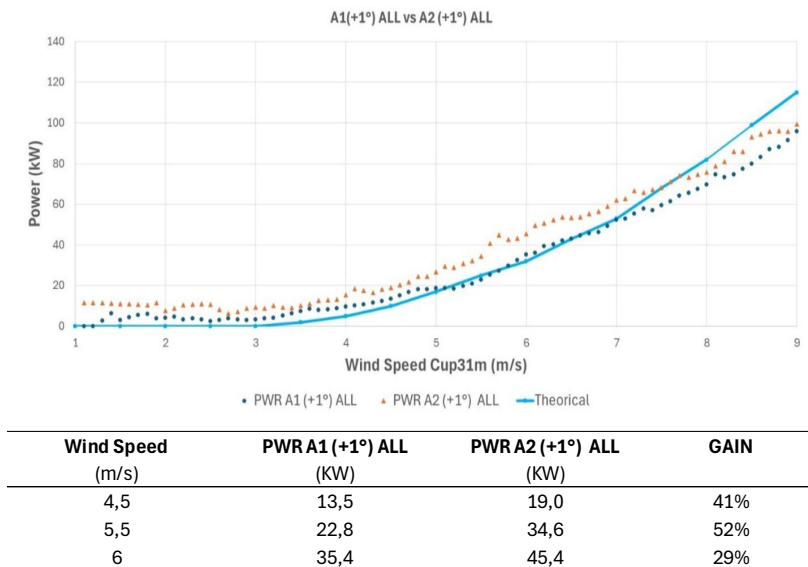
Figure 12 - A1(pitch +1°) & A2(pitch +1°) power curve filtering according to the Attached / Detached criteria

225   And when A1 is optimized with R9 attached on A1, it produces as much as A2 (figure 13). This confirms that A1 production is not optimized as A2.

Wind Speed	PWR A1 (+1°) ATTACHED	PWR A2 (+1°) ALL	GAIN
(m/s)	(KW)	(KW)	
5,1	31,6	29,6	7%
5,4	39,1	32,1	22%
7,5	62,1	68,2	-9%
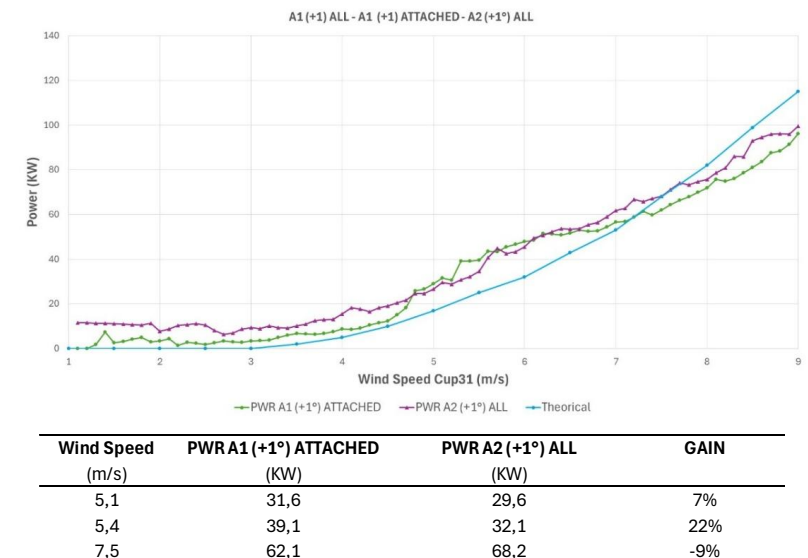
Figure 13 - A1(pitch +1°) & A2(pitch +1°) power curve filtering according to the Attached / Detached criteria

230   This confirms that a pitch control strategy searching for attached R9 just before hard stall behavior will produce the maximum power as seen in the range 4.7-7.5 m/s. The wind speed of 7,5 m/s seems to be the Cp_{max} value of the Vestas V 27 wind turbine. After 7,5 m/s R9 is established in hard stall and there is no more power to gain for this set point where the pitch is fixed to 1°.

As soon as the turbine performances are set for a fixed pitch angle (+1°), we have tested different pitch angles for
235 A1 from -3° to +5° to find potential increase of production. Results showed that for a pitch value of -3° for A1
shows the highest production performance, better than A1 at +1°. Pitch angle of -3° proves to provide a better Cp
than 1° of pitch angle. A1 pitched at -3° produces also more than A2 at +1° (Figure 14).

Wind Speed	A1 (-3°) ALL	A1 (+1°) ALL	GAIN
(m/s)	(KW)	(KW)	
5,4	42,1	20,8	102%
6,8	62,3	46,2	35%
8,1	80,1	74,6	7%
8,6	93,4	83,2	12%
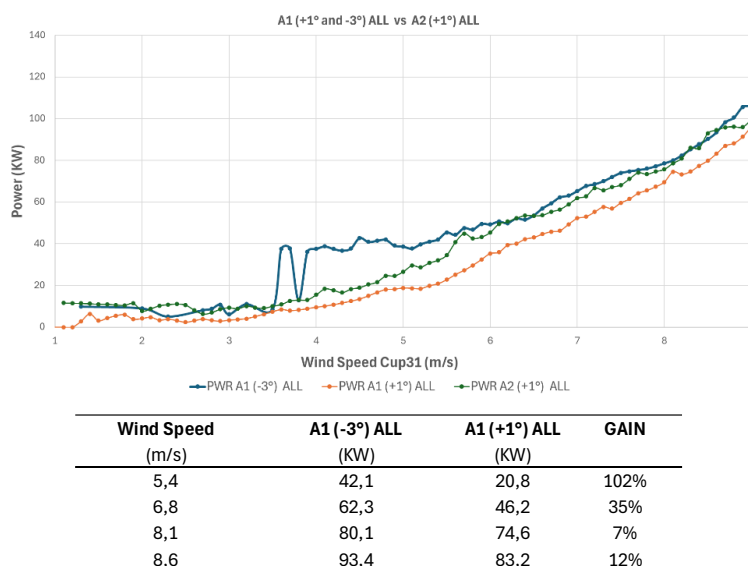
240 **Figure 14 - A1 (pitch +1° and -3°) and A2 (pitch +1°) power curve filtering according to the Attached / Detached**
criteria

Looking at the rotational speed (figure 15), we can see that A2 at 1° is faster than A1 at 1°. And A1 at -3 deg is
much faster than A1 and A2 and it reaches constant rotational speed (rated speed) sooner at 6 m/s than A1 and A2
at 1° reaching rated speed at 10 m/s. Which confirms the better performance of A1 pitched at -3° than the
245 manufacturer set point of 1° of pitch. The rated rotational speed is 0,7 rad/s which correspond to the 43 rpm.
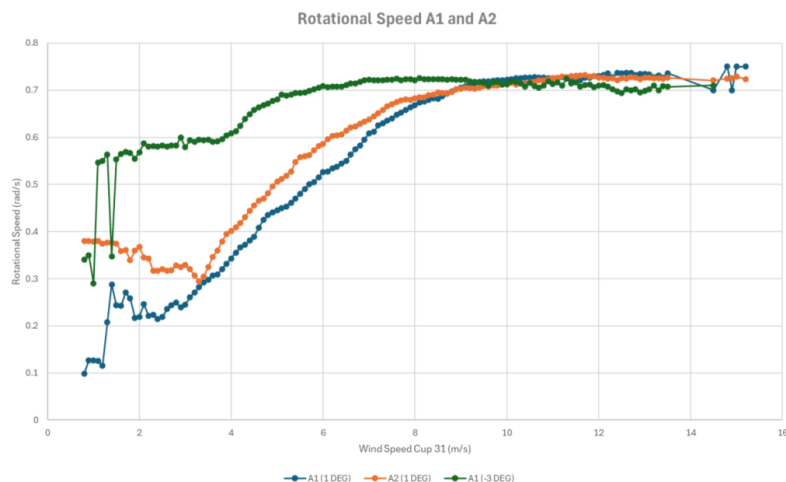
Figure 15 – Rotor speed function of Cup31 for A1 and A2

3.3 Literature review of the Vestas V27 Power curve and Power Coefficient (Cp) curves

To optimize the energy extracted from the wind, the rotor should ideally be operated at a TSR of 8 with a pitch
250 angle of -4° (Varpe, S.A, 2008). Operation at this TSR and pitch will result in the highest Cp (Cp$_{max}$).
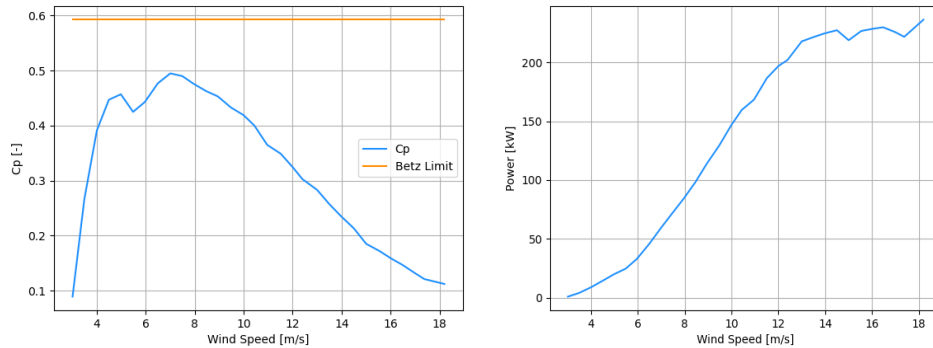
Figure 16 - Vestas V27 characteristics (extracted from the NREL Wind turbine models Power curves archive)

According to the Vestas V27 characteristics extracted from the NREL Wind turbine models power curves archive
(Figure 16), the maximum Cp (Cp$_{max}$) is obtained for a wind speed of v = 7.5 m/s. While the rated power (maximum
255 power) is obtained for a wind speed v= 11 m/s.

Therefore, the Vestas V27 control algorithm will vary the rotating speed with a constant pitch value of 0° to keep
the optimum Lambda up to wind speed v= 11 m/s while the Cp$_{max}$ is attained for v= 7,5 m/s. These results confirm
the experimental result that there is no more power to grab after v=7,5 m/s for a pitch value of 0° (1° for SNL
experimentation).

260 The Vestas V27 should keep constant rotational speed from v=14 m/s which is the rated set point. Experimental
values show constant rotating speed for A1 and A2 from 11 m/s (Figure 15).

Moreover, we see that the Cp$_{max}$ is reached for v = 7.5 m/s. Cp is not maximum before and after this value. The
rated power does not correspond to the maximum power from which rotational speed is kept constant.

Therefore, as soon as Cp$_{max}$ is attained for v=7,5 m/s, there is potential increase of Cp before and after v = 7.5 m/s.

265 And according to (Varpe, S.A, 2008), to improve the Vestas V27 control algorithm, the optimum pitch angle for
the TSR=8 is Theta= -4°. These results are confirmed by the experimentation results where we found the major
potential increase (before 11 m/s) with a pitch angle of -3° with a reference at 1° corresponding to the -4° with
reference at 0°.

3.4 Discussion on eTT R6 and R9 for A1 & A2

270 Figure 17 is a representation of the power curve with a color mapping of the eTT standard deviation (std Bz) to
detect detached and attached behavior of the flow (GenPwr_cor function to wind speed (Cup31m) with a yaw
misalignment filter of -20° to 20° and Blade Pitch filter of 0.9° to 1.1°).

We can note that

- A1R9 predominantly is detached between 4 m/s and 6.5 m/s while A2R9 is attached in all the wind speed
275   ranges

- A2R6 is detached from 5 m/s while A1R6 is detached from 7m/s

Therefore, it confirms that A1 is not optimized through R9 is predominantly stalling. A control strategy looking for R9 attached should provide better production performance as we can see for A2.

A2 at +1° and A1 at -3° seems to have their full potential of production when R6 is stalled while R9 is attached.

280 Therefore, the control strategy should consider R6 stall and R9 attached behavior and avoid R9 chaotic behavior (hard stall) to maximize production.

Therefore, a strategy setting a minimum and a maximum standard deviation for eTT at 15% chord (R6) and eTT at 45% chord (R9) will provide the right measures to detect the optimum angle to maximize production and minimize peak loads by avoiding hard stall.
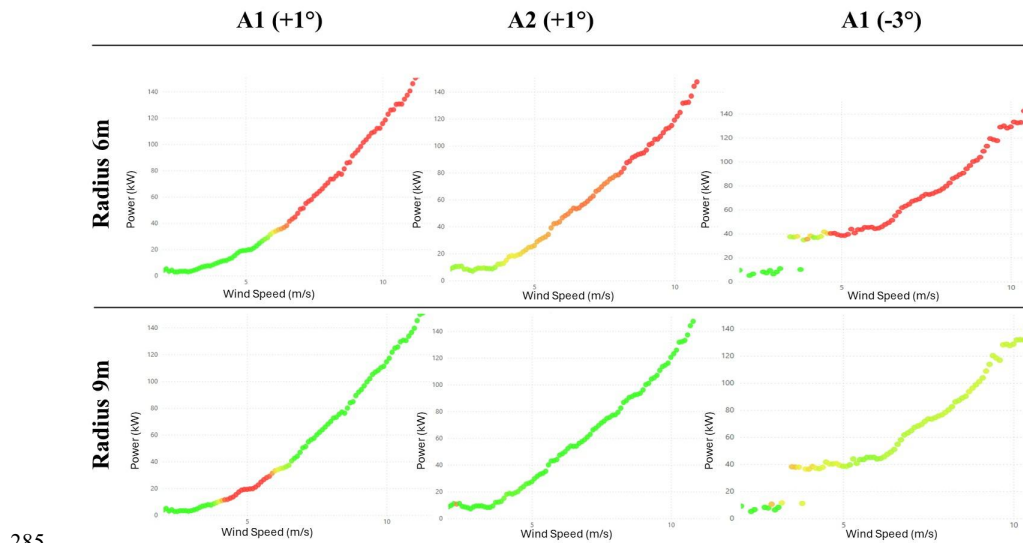
285

Figure 17 - Power Curve function of wind speed with std Bz filter to detect flow behavior (Yaw Misalignment filter - 20° to 20° - Pitch filter 0.9° to 1.1°)

3.5 Remark on the Pitch Regulation for A1 and A2

We note (figure 15) that rotor speed for A2 is more important than for A1 in the range 4 to 8 m/s and the power

290 curves are different between the two wind turbines: A2 produces more than A1.

Theoretically both wind turbines are similar in blade geometry and in control parameters.

If we look at the regulation of the pitch angle (figure 18 and 19), we can see that the amplitude of regulation between A1 and A2 is very different. For A1, the angle goes from 0.5° to 1.5°, while A2 goes from 0.97° to 1.03°. It is also confirmed by the distribution of pitch angles during the test.

295 We can say that the control between A1 & A2 is not similar which could explain the differences of performance between both wind turbines.
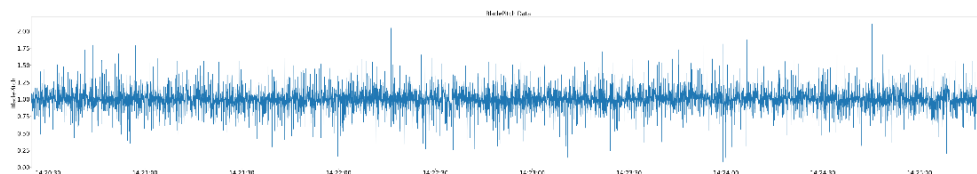
Figure 18 - Example of pitch regulation on A1 (See appendix to get additional time series curve)
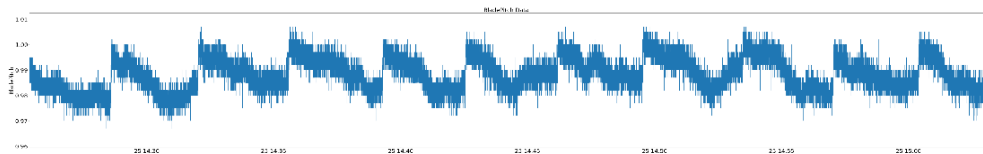
300 **Figure 19 - Example of pitch regulation on A2 (See appendix to get additional time series curve)**

3.6 Pitch offset Trim recommendations

By measuring an AoA on blades at radius 6m for a range of wind speed, it is possible to propose a pitch offset recommendation function of wind speed to get the same AoA on the three blades (table 1). The goal is to reduce

305 aerodynamic unbalance at all wind speed range.

The recommendations is the average of all blades at R6 for a specific wind speed range.

The added value of this method is to provide recommendations in function of the wind speed.

The first thing to note is that the offset of A1 and A2 are different on Radius 6 m.

The average offset for A2 is decreasing with the wind speed range from 22.72° to 20.69°. We don't observe the

310 same decrease on A1.

WindSpeed 4-5 m/s

	A1(BladeA)	A1(BladeB)	A1(BladeC)	Average All Blade
AoA for pitch +1°	**18,60°**	**17,83°**	**17,68°**	**18,02°**
Deviation From Average	0,58°	-0,19°	-0,34°	

WindSpeed 5-6 m/s

	A1(BladeA)	A1(BladeB)	A1(BladeC)	Average All Blade
AoA for pitch +1°	**12,75°**	**11,31°**	**10,04°**	**11,36°**
Deviation From Average	1,39°	-0,05°	-1,32°	

WindSpeed 6-7 m/s

	A1(BladeA)	A1(BladeB)	A1(BladeC)	Average All Blade
AoA for pitch +1°	**2,26°**	**3,49°**	**1,98°**	**2,58°**
Deviation From Average	-0,32°	0,91°	-0,60°	

WindSpeed 4-5 m/s

	A1(BladeA)	A1(BladeB)	A1(BladeC)	Average All Blade
AoA for pitch -3°	**16,16°**	**17,31°**	**16,41°**	**16,63°**
Deviation From Average	-0,47°	0,68°	-0,22°	

WindSpeed 5-6 m/s

	A1(BladeA)	A1(BladeB)	A1(BladeC)	Average All Blade
AoA for pitch -3°	**16,82°**	**17,20°**	**16,45°**	**16,82°**
Deviation From Average	0,00°	0,38°	-0,37°	

WindSpeed 6-7 m/s

	A1(BladeA)	A1(BladeB)	A1(BladeC)	Average All Blade
AoA for pitch -3°	**17,05°**	**17,04°**	**16,37°**	**16,80°**
Deviation From Average	0,25°	0,24°	-0,43°	

WindSpeed 4-5 m/s

	A2(BladeA)	A2(BladeB)	A2(BladeC)	Average All Blade
AoA for pitch +1°	**25,19°**	**22,42°**	**20,37°**	**22,72°**
Deviation From Average	2,47°	-0,30°	-2,35°	

WindSpeed 5-6 m/s

	A2(BladeA)	A2(BladeB)	A2(BladeC)	Average All Blade
AoA for pitch +1°	**23,60°**	**21,15°**	**19,71°**	**21,56°**
Deviation From Average	2,04°	-0,41°	-1,85°	

WindSpeed 6-7 m/s

	A2(BladeA)	A2(BladeB)	A2(BladeC)	Average All Blade
AoA for pitch +1°	**21,53°**	**20,50°**	**19,95°**	**20,69°**
Deviation From Average	0,84°	-0,19°	-0,74°	

315   **Table 1 - Pitch offset recommendation function of wind speed**

3.7 CN function of pitch angle

The Normal (to the chord) lift coefficient CN is estimated with eTT raw data, rotor speed and wind speed by applied mathematical model and a trained with data from wind tunnel. Figure 20 represent CN function of the pitch angle for each blade. Colours represent the standard deviation of eTT raw data (green= attached red =

320 detached).

The CN is increasing from pitch +3° to pitch -2°. Each pitch angle offset is well drawing on CN for A1.
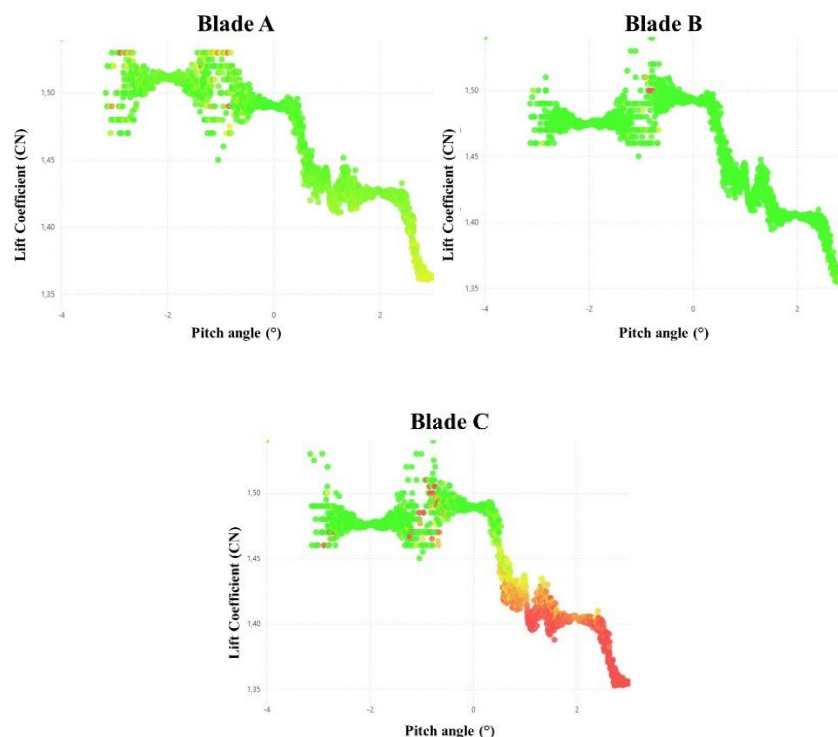
Figure 20 - Coefficient CN for A1 blade A B and C (Wind Speed 2m/s to 8m/s)

4   Conclusions

325

In this paper we present the testing of a method to qualify the power curve in terms of detached and attached moment. The results demonstrate the ability of the eTT sensor to detect the under production of a wind turbine and the machine learning algorithm to detect blade misalignment. The results also demonstrate the potential gain from real time flow monitoring to get a maximum of attached flow on the blade.

330 The aerodynamic eTT sensors placed on each blade of 2 wind turbines (Vestas V27 - 225kW) showed that when the flow is attached, the production is 15% higher than average, and conversely when the flow is detached, production falls by 30%. Hence, the state-of-the-flow measured on the blades has a high correlation with the output power and loads.

The approach was made possible by applied mathematical tools to link the eTT signals on a 2D model full scale

335 blade in the CSTB high speed wind tunnel to lift coefficient and angle of attack (AoA). The research quantifies the effect of aerodynamic behaviour on the wind turbine electric power production. The Power Loss criteria is considered to prove that eTT raw data is highly correlated with the output power of the wind turbine.

The SWIFT Facilities gives the opportunity to have access to high frequency meteo mast data (True Wind Speed, True Wind Direction, Pressure, Temperature and Relative Humidy). The correction of generated power is possible

340 to get a GenPower corrected on each wind turbine.-At the same time, the eTT sensors provide raw data on 5 positions on the blade's suction side in such a way that it is possible to differentiate the Corrected GenPower curve in detached and attached behaviours.

With this method, we show that during 33% of time, 15% of power (kW) was lost during the test in low and medium winds.

345 A solution to recover this power loss is to implement new control strategies for wind turbine blades.

A pitch control strategy searching for attached R9 just before hard stall behavior will produce the maximum power as seen in the range 4.7-7.5 m/s for A1, 4.7-6.5 m/s for A2 and confirmed by the convergence of A1 to A2 performance in this range.

- For instance, for A1 at 5.2m/s it is observed that when the flow is attached on eTT R9 the power is 65%
350   higher than for the measured power curve. There is a huge potential (around 59%) of increase power for A1 at +1° of pitch if the flow is attached at R9.
- The power of A1 and A2 wind turbines have been compared to conclude that A2 produces more than A1 for the whole range of wind speed. When A1 has R9 attached the power curve reaches A2 production.
- A2 is producing more than A1 but even for A2 the potential for increased power is huge (e.g. 18% at
355   5.7m/s to 32% at 5.2m/s).
- The test at -3° of pitch for A1 confirms that it is possible to get more with the same wind turbine when the AoA increases to the optimal angle.

To get the maximum of electric power production, the proposed control strategy would focus on tracking the optimum angle of attack (AoA) instead of varying the rotational speed with a constant pitch angle.

360 Moreover, with the same pitch control algorithm, aerodynamic imbalance can be addressed by measuring the AoA on the blade at different radius for a range of wind speed, and providing a pitch offset recommendation function of the wind speed to get the same AoA on the three blades.

In summary with this method, we can address:

365 - Blade Pitch misalignment identification for given wind speed with AoA analysis.
- Optimisation to reach maximum power by static pitch angle to catch the optimum AoA.

Moreover, we showed the potential optimisation to reach maximum power with dynamic pitch control considering the eTT standard deviation for 15% and 45% chord. Testing such new control algorithm will be the subject of a

370 future project.

5   Financial support

This research has been supported by the Total Energies ON Batch#4 program and TotalEnergies R&D department.

6   Acknowledgements

375   The authors would like to thank the technical staff at CSTB who carried out experiments in the high wind tunnel, and the technical team of Sandia National Laboratory to allow the experimental campaign at the SWIFT facilities

7   Competing interests

Didier VELAYOUDON and Dimitri VOISIN has declared to be board members of Blade Sense SAS. Dimitri VOISIN is the inventor of the patent related to the technology described in this article.

380   **References**

Astolfi, D.: A study of the impact of pitch misalignment on wind turbine performance, Machines, 7, 8, https://doi.org/10.3390/machines7010008, 2019.

Bartholomay, S., Michos, G., Perez-Becker, S., Pechlivanoglou, G., Nayeri, C., Nikolaouk, G., and Paschereit, C. O.: Towards Active Flow Control on a Research Scale Wind Turbine Using PID controlled Trailing Edge Flaps,

385   Wind Energy Symposium, American Institute of Aeronautics and Astronautics, Inc., https://doi.org/10.2514/6.2018-1245, 2018. a

Chamorro, L. P., Guala, M., Arndt, R. E. A., and Sotiropoulos, F.: On the evolution of turbulent scales in the wake of a wind turbine model, J. Turbul., 13, 1–13, https://doi.org/10.1080/14685248.2012.697169, 2012. a

Coquelet, M., Lejeune, M., Bricteux, L., van Vondelen, A. A. W., van Wingerden, J.-W., and Chatelain, P.: On

390   the robustness of a blade-load-based wind speed estimator to dynamic pitch control strategies, Wind Energ. Sci., 9, 1923–1940, https://doi.org/10.5194/wes-9-1923-2024, 2024.

Creaby J, Li Y, Seem JE. Maximizing Wind Turbine Energy Capture Using Multivariable Extremum Seeking Control. *Wind Engineering*. 2009;33(4):361-387. doi:10.1260/030952409789685753

Ezzeddine, W., Schutz, J., and Rezg, N.: Pitot sensor air flow measurement accuracy: Causal modelling and failure

395   risk analysis, Flow, Measurement and Instrumentation, 65, 7–15, https://doi.org/10.1016/j.flowmeasinst.2018.10.021, 2019.

Elosegui, U., Egana, I., Ulazia, A., and Ibarra-Berastegi, G.: Pitch angle misalignment correction based on benchmarking and laser scanner measurement in wind farms, Energies, 11, 3357, https://doi.org/10.3390/en11123357, 2018.

400   GWEC (Global Wind Energy Council) (2025) Global Wind Report 2025. Global Wind Energy Council, Brussels.

Hyers, R., McGowan, J., Sullivan, K., Manwell, J., and Syrett, B.: Condition monitoring and prognosis of utility scale wind turbines, Energ. Mater., 1, 187–203, https://doi.org/10.1179/174892406X163397, 2006.

Kumar, D.; Rotea, M.A. Wind Turbine Power Maximization Using Log-Power Proportional-Integral Extremum Seeking. Energies 15, 1004. https://doi.org/10.3390/en15031004, 2022.

405   Kusnick, J., Adams, D. E., and Griffith, D. T.: Wind turbine rotor imbalance detection using nacelle and blade measurements, Wind Energy, 18, 267–276, https://doi.org/10.1002/we.1696, 2015.

Linyue Gao, Shu Yang, Aliza Abraham, Jiarong Hong, Effects of inflow turbulence on structural response of wind turbine blades, Journal of Wind Engineering and Industrial Aerodynamics, Volume 199, 2020, 104137, https://doi.org/10.1016/j.jweia.2020.104137.

410 Neunaber, I., Danbon, F., Soulier, A., Voisin, D., Guilmineau, E., Delpech, P., … Braud, C. (2022). Wind tunnel study on natural instability of the normal force on a full-scale wind turbine blade section at Reynolds number 4.7 · 106. Wind Energy, 25(8), 1332–1342. https://doi.org/10.1002/we.2732

Soulier, A., Braud, C., Voisin, D., and Danbon, F.: High-Reynolds-number investigations on the ability of the full-scale e-TellTale sensor to detect flow separation on a wind turbine blade section, Wind Energ. Sci., 7, 1043–1052,

415 https://doi.org/10.5194/wes-7-1043-2022, 2022.

Saathoff, M., Rosemeier, M., Kleinselbeck, T., and Rathmann, B.: Effect of individual blade pitch angle misalignment on the remaining useful life of wind turbines, Wind Energ. Sci., 6, 1079–1087, https://doi.org/10.5194/wes-6-1079-2021, 2021.

Veers, P., Bottasso, C. L., Manuel, L., Naughton, J., Pao, L., Paquette, J., Robertson, A., Robinson, M., Ananthan,

420 S., Barlas, T., Bianchini, A., Bredmose, H., Horcas, S. G., Keller, J., Madsen, H. A., Manwell, J., Moriarty, P., Nolet, S., and Rinker, J.: Grand challenges in the design, manufacture, and operation of future wind turbine systems, Wind Energ. Sci., 8, 1071–1131, https://doi.org/10.5194/wes-8-1071-2023, 2023.

Varpe, S.A.: Control system on a wind turbine, Norwegian University of Science and Technology Department of Energy and Process Engineering, http://hdl.handle.net/11250/235060, 2008